Revised Manuscript - Clean Version Click here to view linked References

https://doi.org/10.1016/j.jclepro.2021.129838

This is the Pre-Published Version.

Static and dynamic behaviors of granular soil reinforced by disposable face-mask chips

Jun-Qi Zhang[1], Xiang Wang[1*], Zhen-Yu Yin[1*], Ningyu Yang[1]

Department of Civil and Environmental Engineering, The Hong Kong Polytechnic University, Hung Hom, Kowloon, Hong Kong, China.

Email: xiang.wang@polyu.edu.hk; zhenyu.yin@polyu.edu.hk

Abstract: The stock of disposable face masks has climbed steadily due to COVID-19, which results in an urgent worldwide environmental problem. This investigation aims to assess the potential of using waste mask chips (MC) as reinforcement in granular soil. To evaluate the mechanical properties of the mask chips - granular soil mixture (MSM), a series of monotonic and cyclic triaxial tests with different confining pressures and MC contents are conducted. Then, the shear behavior of MSM is quantified from both static (strength, stiffness, dilatancy) and dynamic (energy absorption capacity, resilient modulus, deformation) perspectives. Furthermore, based on the static and dynamic indexes, the effects of adding MC into granular soil are comprehensively analyzed. All experimental results indicate that the MSMs exhibit an increase of shear strength and a reduction of shear-induced volumetric dilation, but a decrease in stiffness. The addition of MC also leads to an increase in energy absorption but will not affect the cumulative strain of MSMs. Thus, MC has great potential to be used in the embankment construction of road and railway, backfill or reclamation construction, and so on. In addition, the influence of mask chip content on mechanical behaviors of MSM can be considered in current constitutive models for further engineering calculation and design relating to of MSMs. This experimental study provides a new perspective and thought on the recycling of waste face

© 2021. This manuscript version is made available under the CC-BY-NC-ND 4.0 license http://creativecommons.org/licenses/by-nc-nd/4.0/.

masks in civil engineering.

Keywords: Waste masks; Granular material; Triaxial tests; Static and dynamic characteristics

1 Introduction

Wearing disposable face masks has been proved to be an effective way to reduce the infection of airborne infectious diseases, e.g., SARS, H1N1, and Covid-19. In the background of the global Covid-19 pandemic, the consumption of disposable masks has increased significantly (Karaivanov et al., 2021). It is reported that the global use of face masks is more than 129 billion per month (Prata et al., 2020). Based on the predicted model proposed by Nzediegwu and Chang (2020), more than two hundred thousand tons of face masks are generated around the world each day.

The disposable masks (made of non-biodegradable plastics) take hundreds of years to degrade in the natural environment (Dhawan et al., 2019). Currently, the two major ways to treat disposed masks are sent to landfills and incineration (Saberian et al., 2021). However, the mentioned ways have potential risks. Lightweight masks can be moved easily from landfills in wind and rainwater and decomposed into microplastics to endanger the health of organisms (Fadare and Okoffo, 2020). Moreover, the burning of masks will release a lot of harmful gases. Therefore, it is urgent to find a safe and reliable recycling method for disposable masks.

Besides, waste face masks can be regarded as flexible chips that are often used to improve the properties of granular soil in engineering construction. In general, adding flexible chips into granular soil leads to an increase in energy dissipation capacity (Fathali et al., 2017; Sol-Sánchez et al., 2015). Flexible chips are also helpful to protect soil particles from breakage and reduce the dilatancy of granular soils during shear (Buddhima et al., 2018; Gong et al., 2019). Moreover, the additional flexible chips into granular soil have the advantage of decreasing the concentration of contact forces under external loading (Guo et al., 2020; Zhang et al., 2020c). Along this way, waste masks are supposed to be more suitable for improving the engineering properties of granular soils. However, the engineering properties of flexible chips reinforced soil highly relate to the materials. For example, Mashiri et al. (2015) concluded that the additional flexible chip leads to the increasing strength of granular soil, but Lee et al. (2014) indicated that the strength of granular soil decreases with increasing flexible chip content. In addition, Fathali et al. (2017) found that adding a small number of flexible chips can reduce the settlement of granular soil under cyclic load, but this phenomenon was not found in the study of Qi et al. (2018). Thus, understanding the effect of the waste mask on granular soil is important to evaluate the potential of the waste mask as a geo-material, since the mask chips are different from currently used fiber or rubber based chips in term of tensile strength and contact area.

This study aims to assess the potential of using waste masks in reinforcing granular soils. Graded crushed rock particles, one of the most widely used granular soil in civil engineering, is used to blend with waste masks. First, a series of monotonic and cyclic triaxial tests are conducted to investigate the improvement in the performance of granular soil by adding waste masks under different mask contents. Then, the results of the monotonic triaxial tests, including the stress-strain behavior and volume change, are quantified. Finally, the evolution of energy absorption, resilient modulus, and cumulative deformation is analyzed through cyclic triaxial tests.

2 Laboratory Testing Program

2.1 Tested materials

In this investigation, the adopted granular soil, well-graded limestone, was sampled from a quarry in Changsha, China. Moreover, the disposable face masks in this study were produced by Nanchang Jiangnancheng Medical Instrument Co., Ltd. Blending entire masks with graded crushed stone is a convenient way to consume the waste face masks. However, the size of masks is too large for traditional geotechnical tests considering the size effect. Thus, as shown in Fig. 1a, the masks were cut into pieces (mask chips) and kept a similar aspect ratio as the entire masks. Correspondingly, as shown in Fig. 1b, the size of granular soil was reduced. The railway subballast (Zhang, 2020), a kind of graded crushed stone with the most stringent demands, was used as the standard in scaling. The ratio of the width of mask chip to d_{50} of scaled granular soil is 20, which is equal to the ratio of the width of entire masks to d_{50} of traditional subballast. Moreover, the specific gravity of adopted granular soil and mask chip are 2.67 and 0.59, respectively.

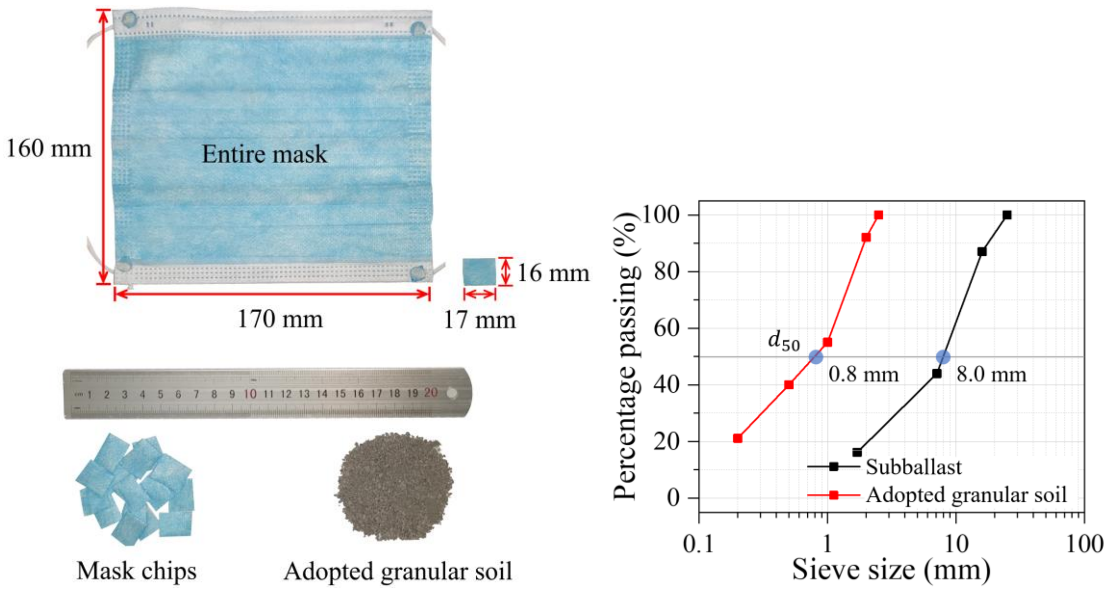

(a) (b)

Fig. 1 Tested materials: (a) photograph and (b) particle size distribution

The masks pieces can be regarded as a special fiber (Bordoloi et al., 2017). For the optimal fiber content of fiber-reinforced soils obtained by previous investigations, Salah et al. (2010) and Chen et al. (2015) suggested that the optimum fiber volumetric content in fiber-reinforced soils is 1.0% (approximately equivalent to 0.5% by weight) considering the increasing shear strength. Fardad Amini and Noorzad (2018) reported that the optimum fiber mass content is 1.0% based on the maximum energy dissipation capacity. Talal (1986) and Gopal et al. (1996) indicated that sand stabilized with fiber mass contents >2% achieved no added benefits. Thus, four mask contents (0%, 0.5%, 1.0%, 1.5%) by weight of dry soil are selected in this study. Moreover, the maximum dry density test of mask chips - granular soil mixture (abbreviated as MSM) is conducted by surface vibration compaction. The maximum dry densities of MSM with 0 % and 1.5 % MC content are 2.04 g/cm^3 and 1.98 g/cm^3, respectively. An increase in MC content leads to an approximately linear decrease in the maximum dry density of MSMs.

The reinforcement effects of chip on soil highly relate to their tensile behaviors. As shown in Fig. 2(a), the tensile test of MC is repeated five times by a high precision tension testing system (MTS insight 30). The width and length of the mask chip in the tensile test are 10 mm and 48 mm, respectively. The results of the repetitive test are similar. Thus, a typical curve is selected to highlight the tensile properties of MC. As shown in Fig. 2(b), the force-displacement curve of MC gradually increases to a long plateau, indicating that MC has excellent toughness. Moreover, the strength of the melt-blown layer (middle layer) is smaller than that of the non-woven layer (outer layer). This phenomenon leads to a sudden drop of the force-displacement curve. In summary, the average strength of MC is 16.2 N based on the five repetitive tests.

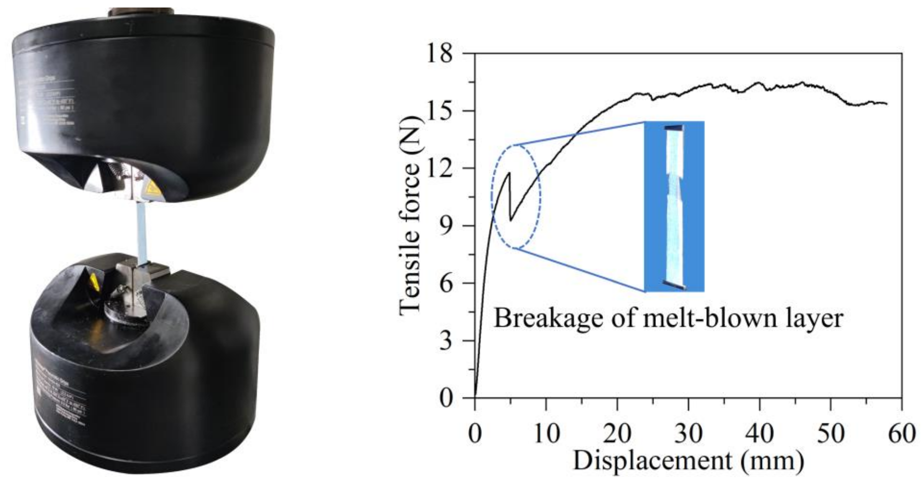

(a) (b)

Fig. 2 Tensile test of mask chip: (a) loading system and (b) test results

2.2 Test procedure and plan

A series of drained monotonic and cyclic triaxial tests were carried out to investigate the static and dynamic characteristics of the MSMs according to ASTM D7181 (ASTM-Standards, 2020) and ASTM D5311/D5311M (ASTM-Standards, 2013), respectively, following four stages: sample preparation, saturation, consolidation, and shearing.

For the stage of sample preparation, the straightforward compaction degree (defined as the target dry density divided by the maximum dry density) was used to quantify the relative compaction level; this method was also used in a previous laboratory investigation and field design of graded crushed stone (Tatsuoka and Gomes Correia, 2018). The specimens were compacted in three layers and were 50 mm in diameter and 100 mm high. All the samples tested in this investigation were prepared with a target compaction degree of 90%. Then, the saturation stage was conducted on the triaxial apparatus and stops when b value (the ratio of the increment of confining pressure to pore pressure) exceeds 95%.

During the shearing stage, monotonic shearing was conducted with a constant strain rate of 0.01 mm/min to ensure that fully drained conditions were maintained during shearing, and shearing was completed when 20% axial strain was achieved. Three commonly used confining pressures σ_c, e.g., 25 kPa, 50 kPa, and 100 kPa (Lenart et al., 2014), were adopted in the monotonic triaxial test to investigate the strength parameters. For the cyclic triaxial test, a single-specimen staged loading method (Ding et al., 2021) was adopted as shown in Fig. 3. To evaluate the dynamic characteristics of MSM under different traffic loads, the cyclic load σ_d was 50%, 100%, 150%, ..., of the confining pressure in each loading stage, and each loading stage was cycled 10 times. The cyclic triaxial tests were stopped when the axial strain reached 4%. Moreover, based on the suggestions of previous studies (Bian et al., 2016), the frequency adopted in the tests was equal to 1 Hz. Two confining pressures, e.g., 50 kPa and 100 kPa, were selected to observe the effects of confining pressures on dynamic responses.

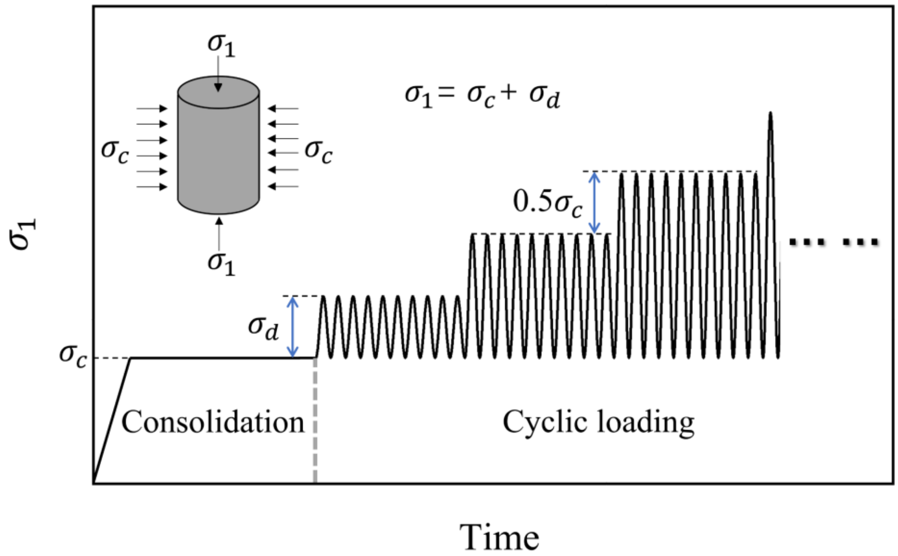

Fig. 3 Load oscillogram for the cyclic triaxial test

All the tested specimens were numbered, and the details of each specimen are summarized in Table 1. The 'C' and 'P' in the name of specimens indicate mass content and confining pressure, respectively. For example, C05P25 is the specimen with 0.5% chip content under confining pressure of 25 kPa. Moreover, the thickness and Young's modulus of membranes are 0.3 mm and 1100 kPa, respectively.

Table 1 Test strategy and basic geotechnical properties of the specimens

Material	Chip content (%)	Triaxial test strategy	σ_c (kPa)	Void ratio
C0P25		Monotonic	25	
C0P50	0	Monotonic and cyclic	50	0.544
C0P100		Monotonic and cyclic	100	
C05P25		Monotonic	25	
C05P50	5	Monotonic and cyclic	50	0.558
C05P100		Monotonic and cyclic	100	
C10P25		Monotonic	25	
C10P50	10	Monotonic and cyclic	50	0.573
C10P100		Monotonic and cyclic	100	
C15P25		Monotonic	25	
C15P50	15	Monotonic and cyclic	50	0.587
C15P100		Monotonic and cyclic	100	

3 Interpretation of Triaxial Tests under Monotonic Loading

To further analyze the results of the monotonic triaxial tests, the axial strain ε_1, deviatoric stress q, effective mean stress p, and stress ratio η are defined as follows:

$$\varepsilon_1 = \frac{h_0 - h}{h_0} \tag{1}$$

$$q = \frac{h\bar{f}}{V} \tag{2}$$

$$p = \sigma_c + q/3 \tag{3}$$

$$\eta = \frac{q}{p} \tag{4}$$

where h_0 and h are the height of the sample before shear (after consolidation) and at present, respectively; V is the current volume of the sample; $\bar{f}$ is defined as the load on the loading plate; and σ_c is the confining pressure.

3.1 Stress-strain relationship

Fig. 4 illustrates the evolution of stress ratio η with shear. η of MSM undergoes a sharp soar to a peak value before expanding gradually to plateau values. The peak and residual strength are similar to previous laboratory investigation of subballast (Suiker Akke et al., 2005), indicating that the adopted crushed stone can reflect the mechanical properties of traditional graded crushed stone.

Fig. 4a indicates that an increase in MC content (*C*) leads to a delayed and indistinct stress peak. The stress-strain relationships of the MCMGs change from a strain-softening type to a strain-hardening type. This phenomenon means that the stress-strain behavior changes from a brittle to a predominantly ductile response with an increasing chip in the skeleton of the specimens. Similar observations have been reported by laboratory and numerical investigations (Kim and Santamarina, 2008; Marandi and Tajabadipour, 2016). Moreover, the addition of mask chips leads to a larger strength because the chip can exert additional tension on the surrounding particles to restrain their movement (Zhang et al., 2020b).

Comparing Fig. 4a, Fig. 4b, and Fig. 4c, with increasing confining pressure σ_c, the stress peak is delayed and gradually disappears. The reasons for this phenomenon are: (1) The instability of the pores increases with the increase in particle contact stress (Zhang et al., 2020a); (2) The surface unevenness of particles decreases under the condition of high local stress, resulting in a decrease in the friction coefficient (Harkness et al., 2016). Compared to low confining pressure conditions (Fig. 4a), the stress curves of specimens with different chip content are similar under high confining pressure (Fig. 4c), indicating that the influence of chip content highly relates to the external load.

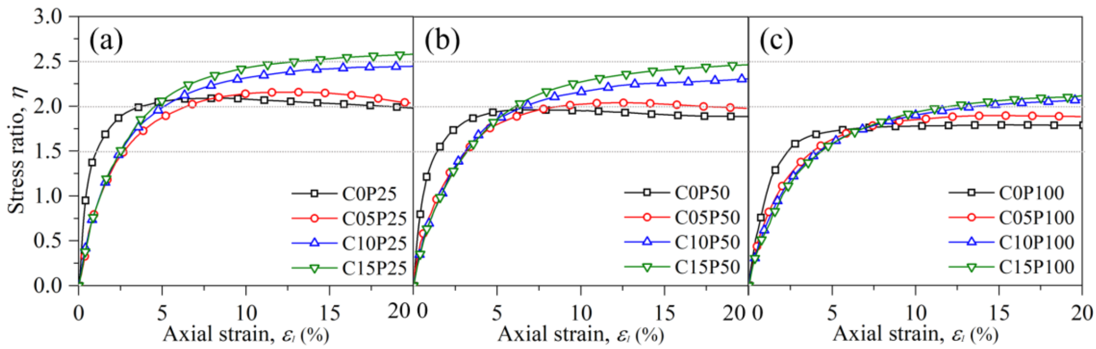

Fig. 4 Stress-strain curves of mask reinforced soil under different confining pressures: (a) 25 kPa, (b) 50 kPa, and (c) 100 kPa

The initial modulus E (defined as the secant modulus at 1% strain) and E_{50} (defined as the secant modulus at 50% strain corresponding to the peak stress) are used to reveal the effect of C on stiffness. To weaken the influence of confining pressure, the initial moduli are expressed in terms of stress ratio and summarized in Fig. 5. As shown in Fig. 5a, the initial modulus drops with increasing confining pressure and chip content. Moreover, the decrease of initial modulus caused by increasing C is highly dependent on the confining pressure; the greater the confining pressure is, the more obvious this decrease. According to the numerical investigation conducted by Zhang et al. (2020b), the particles around flexible chips are easy to rearrange at the beginning of shear because of the deformability of the chip, and an increase in confining pressure leads to the instability of surrounding particles. Interestingly, the increase of confining pressure results in a linear decrease of initial modulus with increasing C. Compared to E, the variation of E_{50} in Fig. 5b has a similar decreasing trend, but the gradient change of E_{50} is not significant. This phenomenon means that the variation of E_{50} highly depends on the delayed peak stress caused by the additional mask chips. It is worth noting that E_{50} of specimens with 1.5% mask content is larger than E_{50} of specimens with 1.0% mask content, indicating that the strain corresponding to the peak stress is much larger than the limitation of the experiment (20% axial strain).

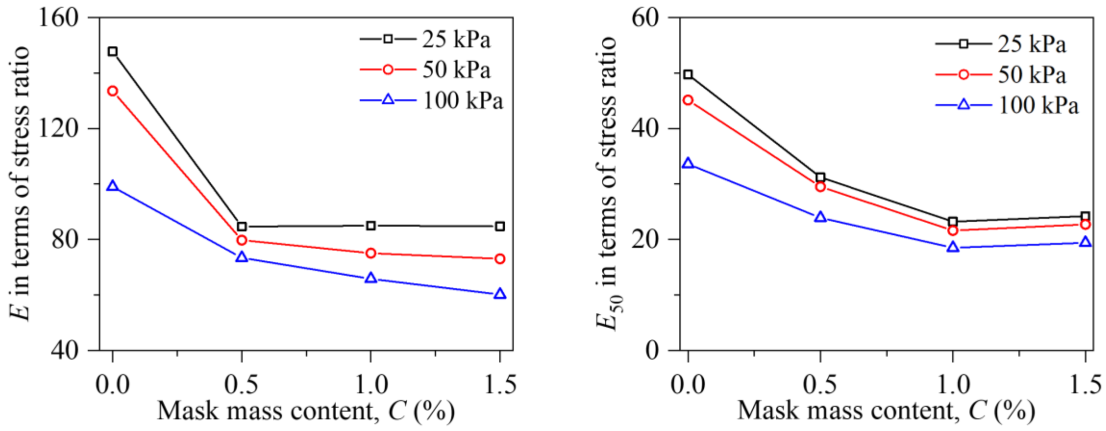

Fig. 5 Summary of the modulus results: (a) *E* and (b) E_{50}

According to the Mohr-Coulomb yielding criteria, the internal friction angle (φ) and the cohesion force (c) of specimens in peak state are obtained for different C. Notably, φ and c of the specimens with 1.5% chip content are not listed because the peak strength of C15P100 and C15P50 was not observed in triaxial tests. Fig. 6 shows the effect of MC content on the φ and c. With increasing MC content, φ increases. According to previous numerical investigation of flexible chip reinforced soil (Zhang et al., 2020b), the flexible chips can restrict the movement of surrounding particles by activating the internal tension, and the restriction is transferred by the friction of the chip-soil interface. Thus, the increasing MC content leads to the increasing φ. Moreover, c is basically constant with increasing MC content.

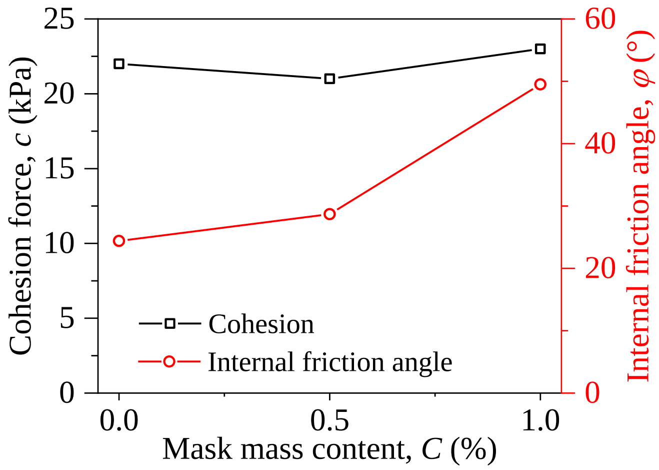

Fig. 6 The internal friction angle and cohesive force of specimens in peak state

3.2 Volumetric strain behavior

In granular materials, the granules slip and rotate with shear, resulting in the volume of the sample changing. The volumetric strain ε_v is used to quantify the volume change of MSMs:

$$\varepsilon_v = \frac{V_0 - V}{V_0} \tag{5}$$

where V_0 and V are the volume of the sample before shear (after consolidation) and at present, respectively.

Fig. 7 illustrates the volumetric strains of MSMs with different *C* under different confining pressures. A positive volumetric strain denotes shrinkage, and a negative volumetric strain denotes expansion. All specimens first undergo a slight contraction and then quickly expand to a stable volume. Increases in confining pressure and chip content will increase shear shrinkage while decrease shear dilatancy, and the axial strain corresponding to the transformation state (the state in which the specimen reaches the zero dilatancy state (Roscoe et al., 1958) during shear) increases. Interestingly, compared to pure crushed stone, the volume change of MSM is less affected by confining pressure.

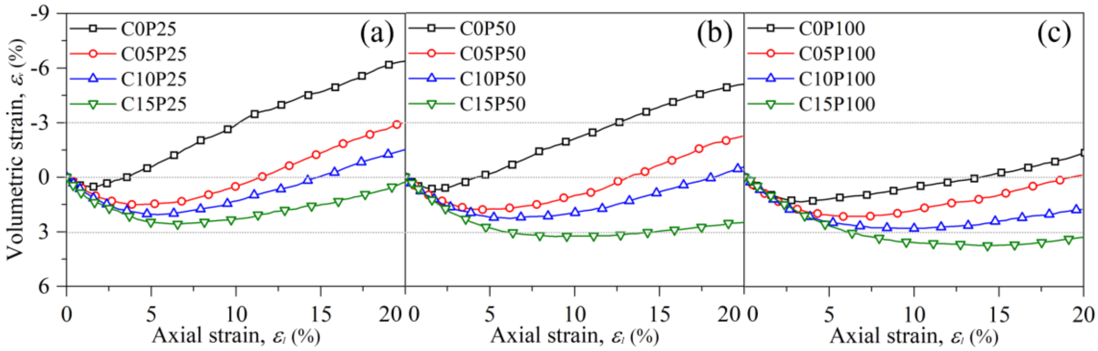

Fig. 7 Effect of chip content on volumetric strain under different confining pressures: (a) 25 kPa, (b) 50kPa and (c) 100kPa

The constitutive model is the basic to predict the engineering properties of soils. The stress-dilatancy relationship is essential for the fundamental constitutive behavior. According to Li and Dafalias (2000), the dilatancy d was quantified as $d\varepsilon_v^p/d\varepsilon_q^p$, where $d\varepsilon_v^p$ and $d\varepsilon_q^p$ denote incremental plastic volumetric strain and incremental plastic deviatoric strain, respectively. The elastic strain is relatively small under adopted confining pressure; thus, $d\varepsilon_v^p$ and $d\varepsilon_q^p$ are assumed equal to incremental volumetric strain and incremental deviatoric strain (Qi et al., 2019), respectively.

Roscoe et al. (1963) assumed that the plastic input work is equal to the dissipated energy. Thus, the dilatancy d under compression condition can be defined as follow:

$$d = M - \frac{q}{p} \tag{6}$$

M is the stress ratio in phase transformation. Because of the discrepancy in fitting experimental tests, a constant D is often introduced to modify the Roscoe' dilatancy (Chang and Yin, 2010; Jefferies, 1993):

$$d = D(M - \frac{q}{p}) \quad (7)$$

Fig. 8a illustrates the stress ratio-dilatancy curves for specimens with σ_c = 50 kPa. The stress ratio-dilatancy curves decrease with increasing stress ratios and turn back at the peak stress. This phenomenon suggests that the stress ratio in the peak state is larger than that in the critical state because the specimens were prepared at a relatively dense state. In addition, as C increases, the dilatancy curve moves up because of the increasing M. It is worth noting that d of all specimens can be well fitted by Eq. (7), and the D of all specimens is basically equal. This indicates that most traditional constitutive models can be directly employed to predict the shear behaviors of MSMs.

The critical state is also an important index for the constitutive model of soils. However, the addition of mask chip delayed critical state; consequently, most specimens did not reach the critical state in triaxial tests. Qi et al. (2019) indicated that the phase transformation state (PTS) influences the critical state of granular materials significantly. Along this way, the phase transformation state lines are plotted in Fig. 8b. For all specimens, the PTS lines exhibit good linearity. In addition, the increasing C leads to the upward movement of the PTS line, and the slope of the curve remains unchanged.

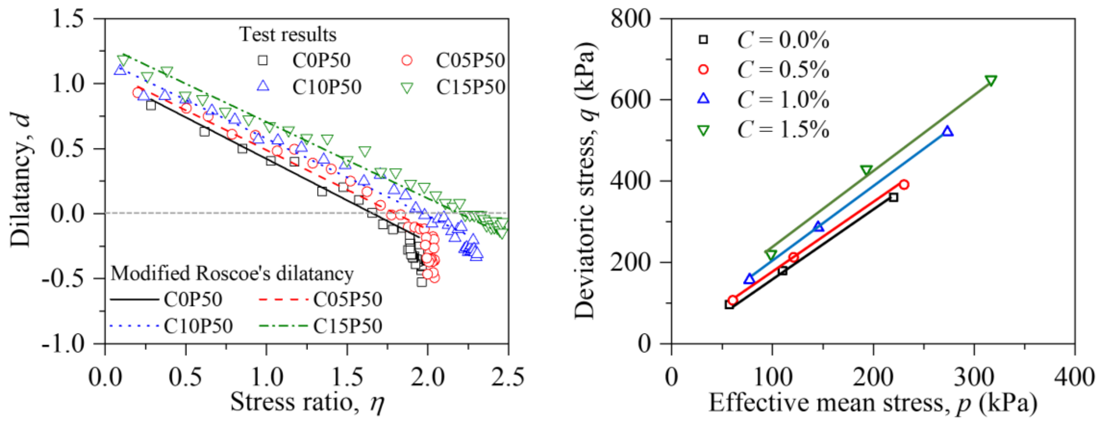

(a) (b)

Fig. 8 Effect of chip content on: (a) stress-dilatancy relationship and (b) phase transformation state line

4 Interpretation of Triaxial Tests under Cyclic Loading

The most unignorable road performance of granular soil in civil engineering is the absorption of transportation vibration. The changes in the transportation vibration energy absorbed by the structural layer, which is consists of granular soil, can be divided into the following three parts (Qi et al., 2018). First, energy is dissipated during the elastic deformation of soil particles. Second, this energy is transformed into internal energy via friction between particles. Third, the transportation vibration energy leads to the movement and breakage of soil particles, resulting in plastic deformation. Therefore, the cyclic triaxial tests are analyzed for three parts, including energy consumption W_D, resilient modulus M_R, and cumulative deformation. The calculation methods of hysteresis loop-related indexes W_D and M_R are listed in Fig. 9. A_{ABC} is the area of the hysteresis loop.

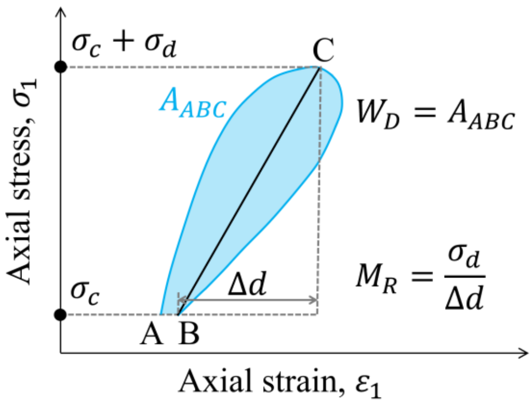

Fig. 9 Calibration of hysteresis loop-related indexes

The hysteresis loop reflects the dynamic properties of unbound road materials directly. Fig. 10a illustrates the hysteresis loops of MSM with different *C* at the last loading stage. With the increase in C, the hysteresis loop gradually inclines to the right, indicating that the rebound deformation increases gradually, which is due to the increase in the elastic deformation ability of MSM due to the addition of the mask chips. The increasing C leads to an increase in the area of the hysteresis loop, indicating that the energy absorption capacity increases with the additional mask chip. Moreover, the change of inclination of the loop is small, indicating that the increasing energy absorption capacity can be attributed to the increasing width of the loop.

Fig. 10b presents the hysteresis loops of C10P50 at N = 15, 25, 35, 45, 55, and 65 (the applied σ_d from 50 kPa to 175 kPa). The width of the hysteresis loop increases with increasing cyclic axial stress, leading to the increase of energy absorption capacity. In addition, the slopes of loops are similar under different cyclic loads, demonstrating that the dynamic properties of MSM are stable under conventional traffic load.

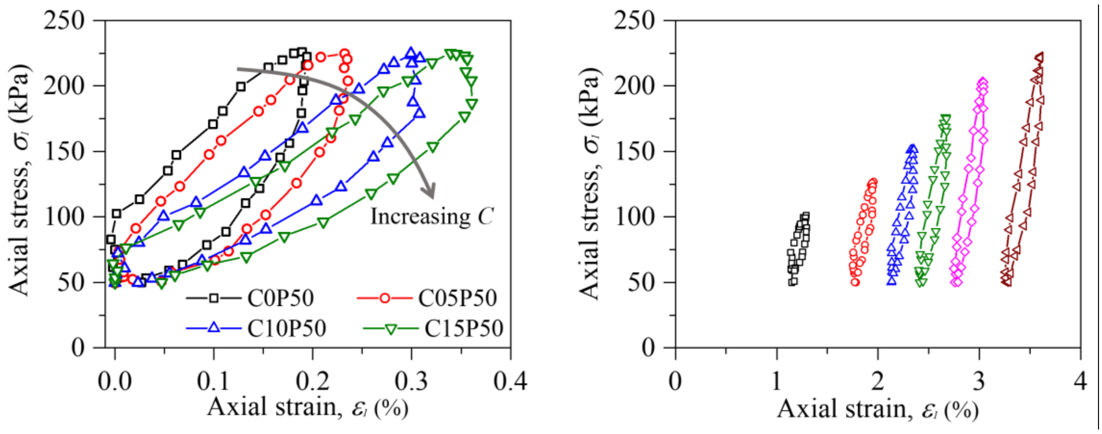

(a) (b)

Fig. 10 Variation of hysteresis loops with: (a) chip content and (b) external load

4.1 Energy absorption

The energy absorption capacity of the structural layer in the road\railway field is significant. Actually, a part of input vibration energy is absorbed by this layer, and others is output to the surface of the subgrade. The increase in the energy absorption capacity of the graded crushed stone layer can significantly enhance the durability of the road structure (Indraratna et al., 2018). The energy consumption W_D in different loading stages are presented in Fig. 11. The value of W_D is the average calculated from the last five hysteresis loops in a specific loading stage. Moreover, the cyclic load σ_d was converted to the stress ratio form to distinguish the effect of confining pressure.

W_D in different loading stages is shown in Fig. 11a to illustrate the energy absorption capacity of MSMs under conventional traffic loads. With increasing η', W_D increases rigidly with increasing gradient. This phenomenon shows that the energy absorption capacity of MSM is extremely sensitive to the external load, indicating that increasing η' leads to wider hysteresis loop, consistent with the variation in the hysteresis loop shown in Fig. 10. Moreover, increasing *C* leads to the monotonic increase of energy absorption capacity of MSM in adopted chip content (0% to 1.5% chip mass content).

Fig. 11b summarizes the energy consumption W_D of each specimen under different confining pressure σ_c. W_D with σ_c = 50 kPa and 100 kPa are marked as black and red lines, and the different cyclic stress ratios are distinguished by different line types. For all samples, W_D increases with increasing mask content, indicating that the additional mask leads to the monotonic increasing of energy absorption capacity of granular soils under conventional load conditions. With increasing σ_c, the energy absorption capacity of all specimens substantially increases for two reasons. One reason is that the input energy of specimen surges. The other reason is that, specimen become denser under a higher confining pressure, leading to the increased number of contact points (Itasca, 2014). Moreover, the distance between black lines is much smaller than that of red lines, suggesting that the effect of confining pressure on low cyclic stress ratio is less than that on high cyclic stress ratio. This result reflects that the width of the hysteresis loop increases with increasing cyclic stress ratio, consistent with the observation in Fig. 10b.

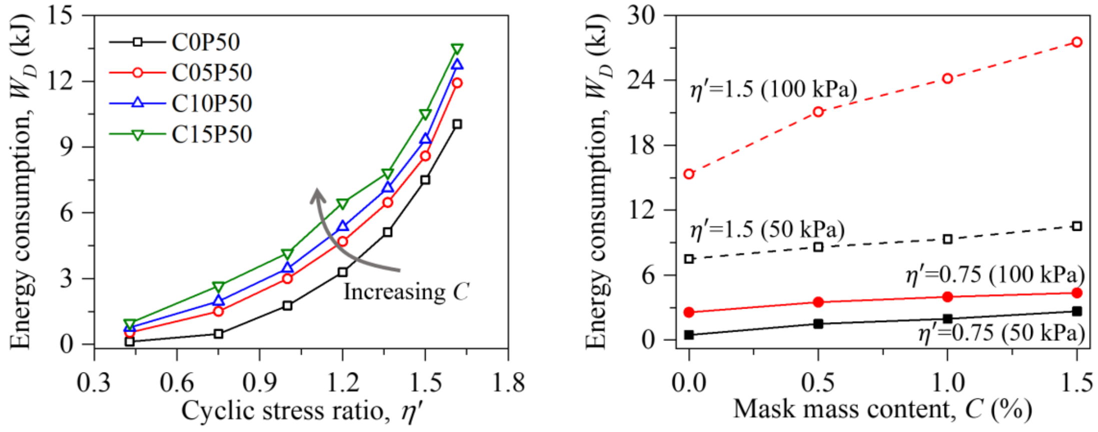

(a) (b)

Fig. 11 Evolutions of energy dissipation W_D with (a) cyclic load and (b) mask content

4.2 Resilient modulus

A large part of the energy input into the structural layer in road\railway field is dissipated by the resilience deformation (Sun et al., 2019), and the resilience deformation can be quantified by the resilient modulus M_R. The value of M_R is also the average calculated from the last five hysteresis loops in a specific loading stage. Fig. 12 illustrates the evolution of the resilient modulus with cyclic loading to investigate the effect of mask content and confining pressure. The relationship between M_R and mask content is explored in Fig. 12. It is observed that, for a specific cycle stress ratio, the M_R value decreases as the mask content increases. Moreover, M_R decreases rapidly in the initial state and expands gradually to plateau values. This phenomenon indicates that the stiffness of MSM will be stable after bearing a certain time under transportation loads and keep constant under conventional stress conditions.

Two typical cyclic stress ratios are selected to investigate the effect of confining pressure, as shown in Fig. 12b. M_R with σ_c = 50 kPa and 100 kPa are marked as black and red lines, and the different cyclic stress ratios are also distinguished by different line types. The black lines are entangled, but an obvious distance between red lines is observed. This phenomenon means that M_R of specimens with η' = 0.75 is not stable; that is, the increasing confining pressure inhibits the time for the specimen to reach stability. Moreover, the larger the confining pressure is, the greater the resilient modulus. Moreover, the resilient modulus of all the samples decreases with increasing *C*. This phenomenon also shows that an increase in *C* leads to a decrease in the stiffness and an increase in the compressibility of MSMs under the same load conditions. Compared to the solid lines, the dotted lines are more linear, indicating that the effect of *C* is related to the external load.

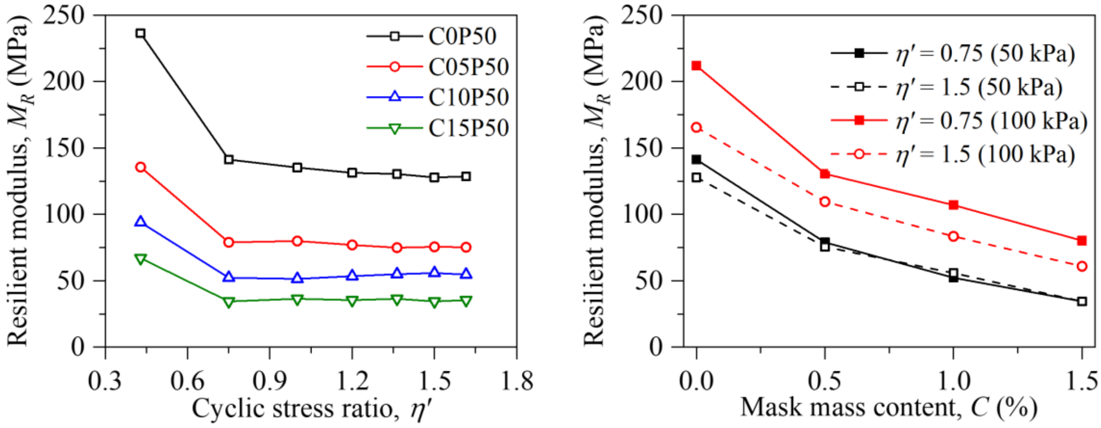

(a) (b)

Fig. 12 Evolution of the resilient modulus with: (a) cyclic load and (b) mask content

4.3 Deformation characteristics

Teixeira et al. (2006) suggested that the deformation of the granular layer is a proper indicator to evaluate the safety of tracks. According to previous investigations of deformation behaviors of granular soils, the settlement mainly occurs in the first few vibrations under a constant cyclic load (Qian, 2014). Thus, even if there are only ten cyclic loads per loading stage, the deformation data is valuable. The evolution of the deformation (expressed as strain) is summarized in Fig. 13. Fig. 13a illustrates the time history curves of specimens with different mask content under σ_c = 100 kPa. For a specific loading stage, the plastic deformation (cumulative axial strain) first increases rapidly and then gradually to a plateau, indicating that the settlement is concentrated in the first vibration. Moreover, in the same loading stage, the bottom of all curves coincides basically, and the top of the curve is quite different. This phenomenon demonstrates that the elastic and plastic deformations caused by the additional mask are inconsistent. The increasing *C* results in a huge increase in elastic deformation and a slight decrease in plastic deformation.

The effects of confining pressure on cumulative settlement are compared in Fig. 13b. The specimens with σ_c = 50 kPa and 100 kPa are marked as black and red lines, and the different mask contents are denoted by different line types. As shown in Fig. 13b, for a specific loading stage, the cumulative axial strain increases with decreasing slope and finally tends to a plateau (named stable state). Moreover, the apparent stable state does not appear in the last few loading stages, indicating that the increasing cyclic stress ratio will inhibit the appearance of a stable state. The black lines are lower than red lines, suggesting that the increase of confining pressure will improve the instability of MSMs. In other words, increasing confining pressure leads to decreasing dynamic strength of MSMs under the same cyclic stress ratios.

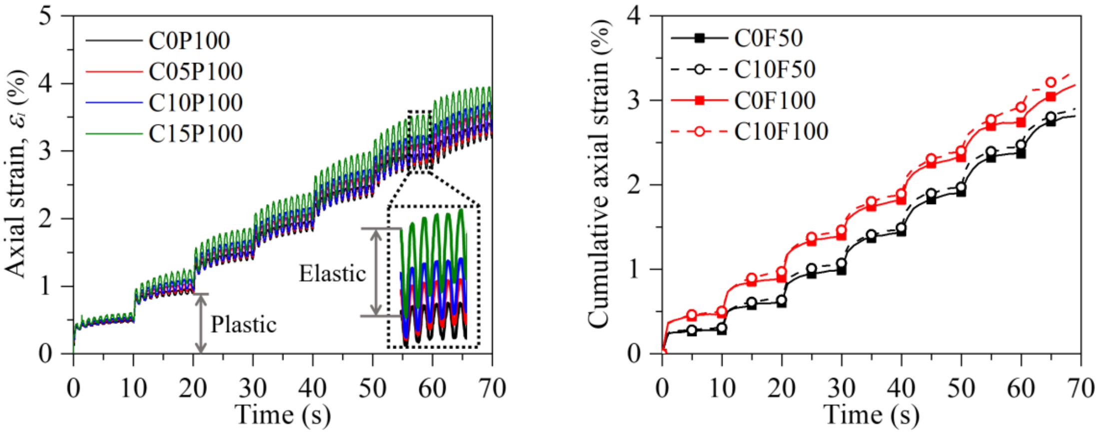

(a) (b)

Fig. 13 Evolution of deformation with number of cycles: (a) effect of mask content and (b) effect of confining pressure

5 Conclusion

By performing a series of monotonic and cyclic triaxial tests, the static and dynamic characteristics of the mask chip-reinforced granular soil (MSM) have been analyzed. Waste face mask has been identified to has a great potential to be used in the road\railway field. The main results can be summarized as follows:

1. Under monotonic loading, the addition of mask chip into the granular soil leads to a decrease in the stiffness, shear dilatancy, delayed peak state, but it increases the strength and internal friction angle.

2. Under cyclic loading, with increasing mask content, the energy absorption capacity substantially increases, and the settlement slightly increases, but the modulus of resilience decreases. Moreover, the increasing energy absorption capacity is due to the increased flexibility.

3. The influence of mask chip content highly relates to the external load. Moreover, there is a great probability that some existing constitutive models can predict the shear behavior of MSMs.

This investigation may promote the application of MC in civil construction and the effective reuse of waste masks. Besides, future work will focus on the interface between cohesive soil and the flexible chip in the perspective of microstructure micromechanics.

Acknowledgments

This research was financially supported by the Research Grants Council (RGC) of Hong Kong Special Administrative Region Government (HKSARG) of China (Grant No.: R5037-18F).

Reference

ASTM-Standards, 2020. Standard test method for consolidated drained triaxial compression test for soils (D7181-20). ASTM Stand. Guid.

ASTM-Standards, 2013. Standard Test Method for Load Controlled Cyclic Triaxial Strength of Soil. ASTM Stand. Guid.

Bian, X., Jiang, J., Jin, W., Sun, D., Li, W., Li, X., 2016. Cyclic and Postcyclic Triaxial Testing of Ballast and Subballast. J. Mater. Civ. Eng. 28. https://doi.org/10.1061/(asce)mt.1943-5533.0001523

Bordoloi, S., Hussain, R., Garg, A., Sreedeep, S., Zhou, W.-H., 2017. Infiltration characteristics of natural fiber reinforced soil. Transp. Geotech. 12, 37–44.

https://doi.org/https://doi.org/10.1016/j.trgeo.2017.08.007

Indraratna, B., Qi, Y., Heitor, A., 2018. Evaluating the Properties of Mixtures of Steel Furnace Slag, Coal Wash, and Rubber Crumbs Used as Subballast. J. Mater. Civ. Eng. 30. https://doi.org/10.1061/(asce)mt.1943-5533.0002108

Chang, C.S., Yin, Z.-Y., 2010. Modeling Stress-Dilatancy for Sand under Compression and Extension Loading Conditions. J. Eng. Mech. 136. https://doi.org/10.1061/(asce)em.1943-7889.0000116

Chen, M., Shen, S.-L., Arulrajah, A., Wu, H.-N., Hou, D.-W., Xu, Y.-S., 2015. Laboratory evaluation on the effectiveness of polypropylene fibers on the strength of fiber-reinforced and cement-stabilized Shanghai soft clay. Geotext. Geomembranes 43, 515–523. https://doi.org/https://doi.org/10.1016/j.geotexmem.2015.05.004

Dhawan, R., Bisht, B.M.S., Kumar, R., Kumari, S., Dhawan, S.K., 2019. Recycling of plastic waste into tiles with reduced flammability and improved tensile strength. Process Saf. Environ. Prot. 124, 299–307. https://doi.org/https://doi.org/10.1016/j.psep.2019.02.018

Ding, Y., Zhang, J., Chen, X., Wang, X., Jia, Y., 2021. Experimental investigation on static and dynamic characteristics of granulated rubber-sand mixtures as a new railway subgrade filler. Constr. Build. Mater. 273, 121955. https://doi.org/https://doi.org/10.1016/j.conbuildmat.2020.121955

Fadare, O.O., Okoffo, E.D., 2020. Covid-19 face masks: A potential source of microplastic fibers in the environment. Sci. Total Environ. 737, 140279. https://doi.org/https://doi.org/10.1016/j.scitotenv.2020.140279

Fardad Amini, P., Noorzad, R., 2018. Energy-based evaluation of liquefaction of fiber-reinforced sand using cyclic triaxial testing. Soil Dyn. Earthq. Eng. 104, 45–53. https://doi.org/10.1016/J.SOILDYN.2017.09.026

Fathali, M., Nejad, F.M., Esmaeili, M., 2017. Influence of Tire-Derived Aggregates on the Properties of Railway Ballast Material. J. Mater. Civ. Eng. 29. https://doi.org/10.1061/(asce)mt.1943-5533.0001702

Gong, H., Song, W., Huang, B., Shu, X., Han, B., Wu, H., Zou, J., 2019. Direct shear properties of railway ballast mixed with tire derived aggregates: Experimental and numerical investigations. Constr. Build. Mater. 200, 465–473. https://doi.org/10.1016/j.conbuildmat.2018.11.284

Gopal, R., M., V.R., D., C.H., 1996. Probabilistic Analysis of Randomly Distributed Fiber-Reinforced Soil . J. Geotech. Eng. 122, 419–426. https://doi.org/10.1061/(ASCE)0733-9410(1996)122:6(419)

Guo, Y., Ji, Y., Zhou, Q., Markine, V., Jing, G., 2020. Discrete Element Modelling of Rubber-Protected Ballast Performance Subjected to Direct Shear Test and Cyclic Loading. Sustain. . https://doi.org/10.3390/su12072836

H., G.D., Talal, A., 1986. Behavior of Fabric- Versus Fiber- Reinforced Sand. J. Geotech. Eng. 112, 804–820. https://doi.org/10.1061/(ASCE)0733-9410(1986)112:8(804)

Harkness, J., Zervos, A., Le Pen, L., Aingaran, S., Powrie, W., 2016. Discrete element simulation of railway ballast: modelling cell pressure effects in triaxial tests. Granul. Matter 18. https://doi.org/10.1007/s10035-016-0660-y

Indraratna, B., Qi, Y., Heitor, A., 2018. Evaluating the Properties of Mixtures of Steel Furnace Slag, Coal Wash, and Rubber Crumbs Used as Subballast. J. Mater. Civ. Eng. 30, 04017251. https://doi.org/10.1061/(asce)mt.1943-5533.0002108

Itasca, 2014. User's manual for PFC3D.

Jefferies, M.G., 1993. Nor-Sand: A simple critical state model for sand. Geotechnique 43. https://doi.org/10.1680/geot.1993.43.1.91

Karaivanov, A., Lu, S.E., Shigeoka, H., Chen, C., Pamplona, S., 2021. Face masks, public policies and slowing the spread of COVID-19: Evidence from Canada. J. Health Econ. 78, 102475. https://doi.org/10.1016/J.JHEALECO.2021.102475

Kim, H.K., Santamarina, J.C., 2008. Sand–rubber mixtures (large rubber chips). Can. Geotech. J. 45, 1457–1466. https://doi.org/10.1139/t08-070

Lee, C., Shin, H., Lee, J.-S., 2014. Behavior of sand-rubber particle mixtures: experimental observations and numerical simulations. Int. J. Numer. Anal. Methods Geomech. 38, 1651–1663. https://doi.org/10.1002/nag.2264

Lenart, S., Koseki, J., Miyashita, Y., Sato, T., 2014. Large-scale triaxial tests of dense gravel material at low confining pressures. Soils Found. 54, 45–55. https://doi.org/https://doi.org/10.1016/j.sandf.2013.12.005

Li, X., Dafalias, Y.F., 2000. Dilatancy for Cohesionless Soils. Geotechnique 50, 449–460. https://doi.org/10.1680/geot.2000.50.4.449

Marandi, M., Tajabadipour, M., 2016. Effect of Rubber Tire Chips-Sand Mixtures on Performance of Geosynthetic Reinforced Earth Walls. Period. Polytech. Civ. Eng. 61. https://doi.org/10.3311/PPci.9539

Mashiri, S., Vinod, J.S., Sheikh, M., 2015. Constitutive Model for Sand–Tire Chip Mixture, International Journal of Geomechanics. https://doi.org/10.1061/%28ASCE%29GM.1943-5622.0000472

Nzediegwu, C., Chang, S.X., 2020. Improper solid waste management increases potential for COVID-19 spread in developing countries. Resour. Conserv. Recycl. 161, 104947. https://doi.org/https://doi.org/10.1016/j.resconrec.2020.104947

Prata, J.C., Silva, A.L.P., Walker, T.R., Duarte, A.C., Rocha-Santos, T., 2020. COVID-19 Pandemic Repercussions on the Use and Management of Plastics. Environ. Sci. Technol. 54, 7760–7765. https://doi.org/10.1021/acs.est.0c02178

Qian, Y., 2014. Integrated computational and experimental framework for the assessment of railroad ballast life-cycle behavior.

Roscoe, K., Schofield, A., Wroth, C., 1958. On The Yielding of Soils. Geotechnique 8, 22–53. https://doi.org/10.1680/geot.1958.8.1.22

Roscoe, K., Thurairajah, A., Schofield, A., 1963. Yielding of Clays in States Wetter than Critical. Geotechnique 13, 211–240. https://doi.org/10.1680/geot.1963.13.3.211

Saberian, M., Li, J., Kilmartin-Lynch, S., Boroujeni, M., 2021. Repurposing of COVID-19 single-use face masks for pavements base/subbase. Sci. Total Environ. 769, 145527. https://doi.org/https://doi.org/10.1016/j.scitotenv.2021.145527

Salah, S., S., N.S., Fadi, F., 2010. Shear Strength of Fiber-Reinforced Sands. J. Geotech. Geoenvironmental Eng. 136, 490–499. https://doi.org/10.1061/(ASCE)GT.1943-5606.0000235

Sol-Sánchez, M., Thom, N.H., Moreno-Navarro, F., Rubio-Gámez, M.C., Airey, G.D., 2015. A study into the use of crumb rubber in railway ballast. Constr. Build. Mater. 75, 19–24. https://doi.org/10.1016/j.conbuildmat.2014.10.045

Suiker Akke, S.J., Selig Ernest, T., Frenkel, R., 2005. Static and Cyclic Triaxial Testing of Ballast and Subballast. J. Geotech. Geoenvironmental Eng. 131, 771–782. https://doi.org/10.1061/(ASCE)1090-0241(2005)131:6(771)

Sun, Q., Indraratna, B., Ngo, N.T., 2019. Effect of increase in load and frequency on the resilience of railway ballast. Geotechnique 69, 833–840. https://doi.org/10.1680/jgeot.17.P.302

Tatsuoka, F., Gomes Correia, A., 2018. Importance of controlling the degree of saturation in soil compaction linked to soil structure design. Transp. Geotech. 17. https://doi.org/10.1016/j.trgeo.2018.06.004

Teixeira, P., Pita, A., Casas-Esplugas, C., Bachiller, A., Robuste, F., 2006. Improvements in High-Speed Ballasted Track Design: Benefits of Bituminous Subballast Layers. Transp. Res. Rec. 1943, 43–49. https://doi.org/10.3141/1943-06

Qi, Y., Indraratna, B., Heitor, A., Vinod, J.S., 2018. Effect of Rubber Crumbs on the Cyclic Behavior of Steel Furnace Slag and Coal Wash Mixtures. J. Geotech. Geoenvironmental Eng. 144. https://doi.org/10.1061/(asce)gt.1943-5606.0001827

Qi, Y., Indraratna, B., Coop, M.R., 2019. Predicted Behavior of Saturated Granular Waste Blended with Rubber Crumbs. Int. J. Geomech. 19. https://doi.org/10.1061/(asce)gm.1943-5622.0001440

Zhang, J., 2020. Investigation of macro- and micro-mechanical properties of waste rubber-cohesionless soil mixtures. Central South University.

Zhang, J., Wang, X., Yin, Z.-Y., Liang, Z., 2020a. DEM modeling of large-scale triaxial test of rock clasts considering realistic particle shapes and flexible membrane boundary. Eng. Geol. 279, 105871. https://doi.org/https://doi.org/10.1016/j.enggeo.2020.105871

Zhang, Junqi, Chen, X., Zhang, Jiasheng, Jitsangiam, P., Wang, X., 2020b. DEM investigation of macro- and micro-mechanical properties of rigid-grain and soft-chip mixtures. Particuology. https://doi.org/https://doi.org/10.1016/j.partic.2020.06.002

Zhang, Junqi, Chen, X., Zhang, Jiasheng, Wang, X., 2020c. Microscopic investigation of the packing features of soft-rigid particle mixtures using the discrete element method. Adv. Powder Technol. 31, 2951–2963. https://doi.org/https://doi.org/10.1016/j.apt.2020.05.019